18TH WORLD CONFERENCE ON EARTHQUAKE ENGINEERING
WCEE2024
MILAN

MILAN, ITALY
30TH JUNE - 5TH JULY 2024
www.wcee2024.it

NONLINEAR MODELLING OF STEEL WIDE-FLANGE COLUMNS: FRONTIERS AND PROSPECTS FOR FUTURE DEVELOPMENTS

O. Moammer[1], A. Imanpour[2] and R. Tremblay[3]

[1] Ph.D. Student, Dept. of Civil and Environmental Engineering, University of Alberta, Edmonton, Canada. E-mail: moammer@ualberta.ca
[2] Associate Professor, Dept. of Civil and Environmental Engineering, University of Alberta, Edmonton, Canada. E-mail: imanpour@ualberta.ca
[3] Professor, Dept. of Civil, Geological and Mining Engineering, Polytechnique Montreal, Montreal, Canada. E-mail: robert.tremblay@polymtl.ca

Abstract: *Steel wide-flange columns of concentrically braced frames (CBF) involving seismic-induced soft-story mechanisms are prone to local instability at their ends and global instability along the member length due to combined effects of axial compression force and flexural bending. These instability modes often occur concomitantly in the nonlinear range of the material. Efficient numerical modelling of this complex response is essential in engineering applications to evaluate the seismic response of existing buildings and design new structures. However, available nonlinear modelling approaches, including the concentrated plasticity approach and distributed plasticity technique, e.g., fibre-based methods, may not adequately capture the inherent cyclic inelastic response of steel CBF columns and their associated instability modes, which can compromise the reliability of the nonlinear analysis in CBF buildings, particularly when columns do not meet member or section slenderness limits implicit in contemporary building codes, e.g., columns of existing CBF buildings. Motivated by the lack of efficient nonlinear modelling techniques for seismic response evaluation of steel CBF columns in engineering applications, this paper aims to first evaluate available nonlinear modelling approaches for the simulation of the stability response of steel wide-flange columns in CBF structures, highlight modelling challenges, and propose recommendations for future development of nonlinear modelling techniques for the simulation of both local and global buckling modes plus their associated axial shortening. The results of this study confirm that the current modelling procedures often used in engineering applications for the nonlinear simulation of steel CBF columns may not be suited to systematically simulate the interactive buckling response expected in steel CBF columns. Proposed recommendations for future advancement of nonlinear modelling techniques demonstrate the potential for overcoming the limitations of the current approaches in predicting the stability limit states of steel CBF columns under seismic loading.*

1 Introduction

Steel wide-flange columns are widely used in the construction of steel concentrically braced frames (CBFs) in seismic-prone regions. Under seismic loading, CBF columns undergo a relatively large axial load, e.g., 90% of the column axial compression capacity, and flexural bending in the plane of the frame. The axial load is produced due to gravity loads and brace axial resistances. Flexural bending is often induced due to relative lateral deformation between adjacent storeys, resulting from uneven distribution of inelastic frame deformation along the frame height (Toutant et al., 2017), which can be exacerbated when a soft-storey mechanism is formed, e.g., in existing CBF structures. The column can also be exposed to in-plane flexural bending due to the moment transferred from beam-to-column and/or corner gusset plate connections. The moment transferred from the beam can be relatively high when the beam is moment-connected to the column (Seki *et al.*, 2022). Under combined axial load and flexure, CBF columns may experience local buckling, near the ends or mid-height of the column, and global or member instability, flexural buckling, flexural-torsional buckling, or lateral-torsional buckling, along the member length due to the combined effects of axial compression force and flexural bending (Newell and Uang, 2008; Lamarche and Tremblay, 2011; Fogarty and El-Tawil, 2016; Auger, 2017; Balazadeh Minouei, 2017). These instability modes often occur concomitantly in the nonlinear range of the material, involving flexural plastic hinging, and cause axial shortening. Several parameters can affect the potential interactive buckling mode and ultimately the failure mode of the column. Among those are the axial load level, axis of bending, section compactness, member slenderness ratio, torsional properties, and boundary conditions. For example, CBF columns undergoing weak-axis bending are unlikely to experience lateral-torsional buckling, or member buckling may not develop in a first-storey fixed-based column due to added stiffness from the base condition.

Numerical modelling of the nonlinear response of steel CBF columns, under high-level of axial load and flexure due to lateral deformation or end rotation, represents a key importance in practice, in particular, in seismic response assessment and rehabilitation of existing steel buildings that suffer deficient structural elements under low-probability occurrence seismic events, e.g., wide-flange columns with slender web and flanges. However, the numerical models implemented in the available structural analysis programs, which are often used in engineering practice, may not have the capacity to simulate the effects of the complex interactive buckling limit states of CBF columns on the seismic response of the structure. For instance, the concentrated plasticity approach used in plastic hinge springs with associated backbone curves incorporated into structural analysis programs such as SAP2000 (CSI Analysis, 2021), Altair S-Frame (Altair Engineering INC, 2023), ETABS (CSI Analysis, 2023), and RFEM (Dlubal Software, 2023) can simulate the influence of local buckling near the end of the member through post-capping stiffness degradation. Nonlinear modelling parameters of such backbone curves, including post-yielding and post-capping stiffness, yielding and capping strengths, and plastic, capping and ultimate rotations, should be obtained based on calibration against experimental test data or be adapted from available database, e.g., those specified in ASCE 41 (ASCE, 2017) and AISC 342 (ANSI/AISCa, 2022). The majority of the plastic hinge models can also account for the determinantal effect of axial compression force on the moment and rotational ductility of steel members (Fogarty and El-Tawil, 2016; Balazadeh Minouei, 2017; Cravero, Elkady and Lignos, 2020). However, these models typically fail to account for the influence of axial shortening, due to local buckling (MacRae *et al.*, 2009), global buckling or interactive local and member buckling (Balazadeh Minouei, 2017), on the member nonlinear response. Fibre discretization of cross-section has recently been implemented in most of the structural analysis programs to allow for distributed plasticity while maintaining the efficiency of the analysis, in particular, when performing dynamic analysis. Although fibre-based models in structural analysis programs perform fairly well in simulating the nonlinear response of planner systems, such as reinforced concrete shear walls, their accuracy and efficiency in reproducing inelastic member buckling of wide-flange columns and associated axial shortening yet remain a challenge.

The current performance-based guidelines, such as ASCE 41 and AISC 342, provide little guidance on nonlinear modelling of steel wide-flange columns of CBFs. Based on ASCE 41, steel CBF columns under combined axial and flexure, with an axial load exceeding 10% of their axial strength, are evaluated as follows: a flexural plastic hinge in a column is deformation controlled for flexural behaviour and if the column limit states involve member buckling, the column is force controlled for flexure. However, these guidelines were in large adapted from the studies conducted on wide-flange columns part of steel MRFs (Lignos *et al.*, 2019), emphasising the need for special nonlinear models for CBF columns. Furthermore, past studies showed that wide-flange columns possess significant rotational capacity before member instability even under high levels

of axial loads (Auger, 2017; Balazadeh Minouei, 2017), emphasising the need for enhanced performance-based modelling and design requirements for these members.

This paper aims to evaluate nonlinear modelling techniques for the simulation of the stability response of steel wide-flange columns of CBF structures in engineering applications. Two virtual test specimens consisting of wide-flange columns expected in new and existing CBF structures are first selected. A three-dimensional finite element model (FEM) of the columns is constructed and verified against the experimental data. The concentrated plasticity-based model (CPM) of the specimens is then developed in the SAP2000 program (CSI Analysis, 2021) using the available modelling techniques often used in practice. The results obtained from the CPM are used to interrogate the key stability response parameters of CBF columns, including moment-rotation response, axial force – flexural bending interaction and axial shortening, and showcase the challenges associated with nonlinear modeling of such columns. A set of recommendations are finally proposed for future advancement of nonlinear modelling of CBF columns to be used in engineering applications for the evaluation of the seismic response of existing steel CBFs and the performance-based design of new CBF structures.

2 Virtual specimens

Two nearly square wide-flange specimens, W310×97 and W310×129, were selected and numerically modelled in the ABAQUS finite element program (Simulia, 2020). The columns ae assumed to be part of a multi-storey CBF as described in Balazadeh Minouei (2017) and are oriented such that in-plane seismic action induces strong-axis bending. The selected cross-sections are made of ASTM A992 steel with the specified yield strength F_y = 345 MPa and meet the section compactness limits corresponding to Class 3 and Class 1 sections, respectively, as per the Canadian steel design standard (CSA, 2019).

The three-dimensional numerical model of the specimens was created using four-node reduced integration shell elements (S4R) with a 25 × 25 mm mesh size. The steel material was defined with Young modulus E = 200 GPa and Poisson's ratio v = 0.3. Material nonlinearity, including kinematic and cyclic hardening, were modelled using Voce-Chaboche (Lemaitre and Chaboche, 1990) plasticity model. The material model is calibrated based on the procedures discussed in Hartloper et al. (2021) with the following parameters: the hardening modulus C = 3378 MPa, the rate of the change of the hardening parameter γ = 20, the initial size of the yield surface F_y = 345 MPa, the maximum amplitude of expansion of the yield surface, Q_∞ = 90 MPa, and the rate of the change of the yield surface b = 12. The global initial out-of-straightness equal to *L/1500* was assigned to the numerical model (Elkady, 2016; ASTM, 2021; ANSI/AISCb, 2022). No local out-of-straightness was assigned to the cross-section elements to achieve a better match between the numerical prediction and the observation from the experiments used to verify the numerical model, which will be described later (Balazadeh Minouei, 2017). The latter assumption is deemed reasonable because CBF columns are generally less prone to local buckling under seismic loading.

The boundary conditions of the model were set to match those of an intermediate-level CBF column in a multi-storey building (Balazadeh Minouei et al., 2017) in the plane and out of the plane of the frame, summery of which shown in Table 1. In the Table 1, the specimens subjected to constant axial load is labeled as "Cont" and "Var" is used to identify those under varying axial load obtained from the cyclic pushover analysis. The strong axis translational degree-of-freedom (DOF) is displacement control at top of all specimens, and a free condition was used for translational DOF along the longitudinal axis at the top end of the columns to allow for axial shortening. The strong axis lateral and longitudinal DOFs at the bottom of all columns are assigned to be fixed. Out of plane translational DOF is fixed at top and bottom of the columns. The rotational DOF in strong axis was restrained at both ends for specimens under constant axial load, while it was set to be displacement control for specimens under varying axial load. A rotationally-free condition was used in weak axis at both ends. Torsional DOFs are fixed at both ends. Summary of loading conditions is shown in Table 1. Two loading conditions were examined: 1) a constant axial compression load of $0.7P_n$ (where P_n is nominal compressive strength of the column based on AISC 360 (ANSI/AISCc, 2022)), representing the envelope of axial forces induced by the braces plus gravity loads, was applied in force control followed by the AISC 341 symmetric cyclic lateral loading protocol (ANSI/AISCd, 2022) applied in displacement control in strong axis; 2) a more realistic varying axial load, representing the axial forces imposed by the braces and gravity load, applied in force control, plus a varying lateral and strong axis rotational loading protocol imposed in displacement control. All histories for the latter were extracted from a computationally-efficient numerical model of a retrofitted 10-story tension-only braced frame subjected to AISC 341 loading protocol at the roof level using a cyclic pushover analysis. The second loading

condition represents a more realistic loading history expected in steel CBFs with the possibility of a soft-storey mechanism. Additional information regarding the CBF structure selected to develop the second set of loading histories can be found in Balazadeh Minouei et al. (2017).

Table 1. Boundary and loading conditions of the virtual specimens.

Specimen	Boundary Conditions		Axial Load
	Bottom	**Top End**	
W310×129-Cont	Lateral: Restrained Longitudinal: Restrained Strong Axis Rotation: Restrained	Lateral: AISC Protocol Longitudinal: Free Strong Axis Rotation: Restrained	Constant with an amplitude of $0.7P_n$
W310×97-Cont	Lateral: Restrained Longitudinal: Restrained Strong Axis Rotation: Restrained	Lateral: AISC Protocol Longitudinal: Free Strong Axis Rotation: Restrained	Constant with an amplitude of $0.7P_n$
W310×129-Var	Lateral: Restrained Longitudinal: Restrained Strong Axis Rotation: From Cyclic Pushover	Lateral: From Cyclic Pushover Longitudinal: Free Strong Axis Rotation: From Cyclic Pushover	From Cyclic Pushover varying between 0 and $0.7P_n$ including a gravity load of $0.27P_n$
W310×97-Var	Lateral: Restrained Longitudinal: Restrained Strong Axis Rotation: From Cyclic Pushover	Lateral: From Cyclic Pushover Longitudinal: Free Strong Axis Rotation: From Cyclic Pushover	From Cyclic Pushover varying between 0 and $0.7P_n$ including a gravity load of $0.27P_n$

The numerical model developed here was verified against the experimental data of Specimen CS5, encompassing a 4 m-long Class 1 W250×101 profile, reported by Balazadeh Minouei (2017). The loading protocol included a constant axial force of $0.7P_n$ plus a symmetric cyclic displacement protocol, including two cycles of 0.375%, 0.5%, 1% and 7% drift ratios imposed in weak axis. Figure 1a compare column top moment normalized by the plastic capacity of the column in weak axis, M_{py}, versus drift ratio, computed as the relative lateral displacement divided by the initial length of the column, predicted by the finite element model developed here to those obtained from the experiment. Figure 1b shows the comparison between the numerical perdition and experimental data for column axial shortening versus drift ratio. A very good match is observed between the numerical prediction and experimental results, suggesting that the numerical model is capable of predicting cyclic and stability response of wide flange columns subjected to CBF like loading protocols. It is significant to note that exclusion of initial local imperfection helped achieve a better prediction of column instability response, including buckled shape and extent of axial shortening at buckling, due to unnoticeable impact of local web and flange buckling on the stability response of seismically-compact Class 1 profiles acting as CBF columns.

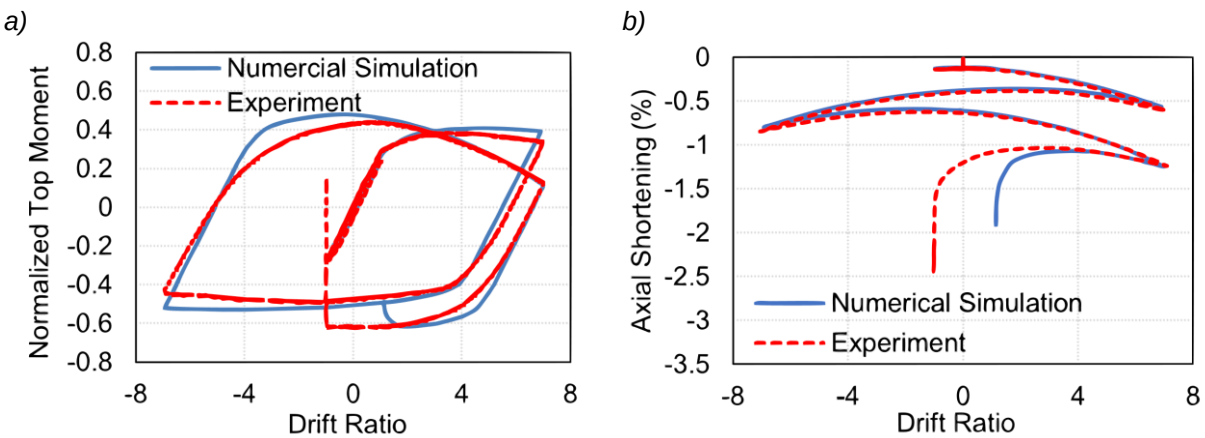

Figure 1. Numerical model validation for a W250×101 under an axial load of $0.7P_n$: a) Top moment vs. drift ratio, b) Axial shortening vs. drift ratio.

3 Stability response of specimens

Figure 2a- 2d show the final deformed shape of the virtual specimens of Table 1 at the point of loss of axial load carrying capacity. The moment – drift ratio response of the virtual specimens is shown in Figure 3a - 3b for the specimens under constant axial load and AISC displacement protocol, and those subjected to varying axial load and lateral displacement and strong axis rotation, respectively. Referring to the moment – drift ratio responses, the value of yielding moment is nearly $M_y = 0.5M_p$ in all specimens when the axial force is maximum. The peak normalized moments reached 0.7 in specimens under fixed axial load; however, the peak moments under compressive forces in the specimens subjected to varying axial load are approximately 1.1 and 1 for W310×129-Var and W310×97-Var, respectively. The effect of the axial load acting on a deformed specimen and local buckling at the ends of the member result in the negative slope in the moment – drift ratio responses shown in Figure 3. For example, the negative slope is dominated by the effect of the axial load in Specimen W310×129-Var during the initial cycles up to 3.3 % drift ratio, local buckling controls the negative slope in Specimen W310×97-Cont, and the combined effects of varying axial load and local buckling dominates the degrading response in Specimen W310×97-Var.

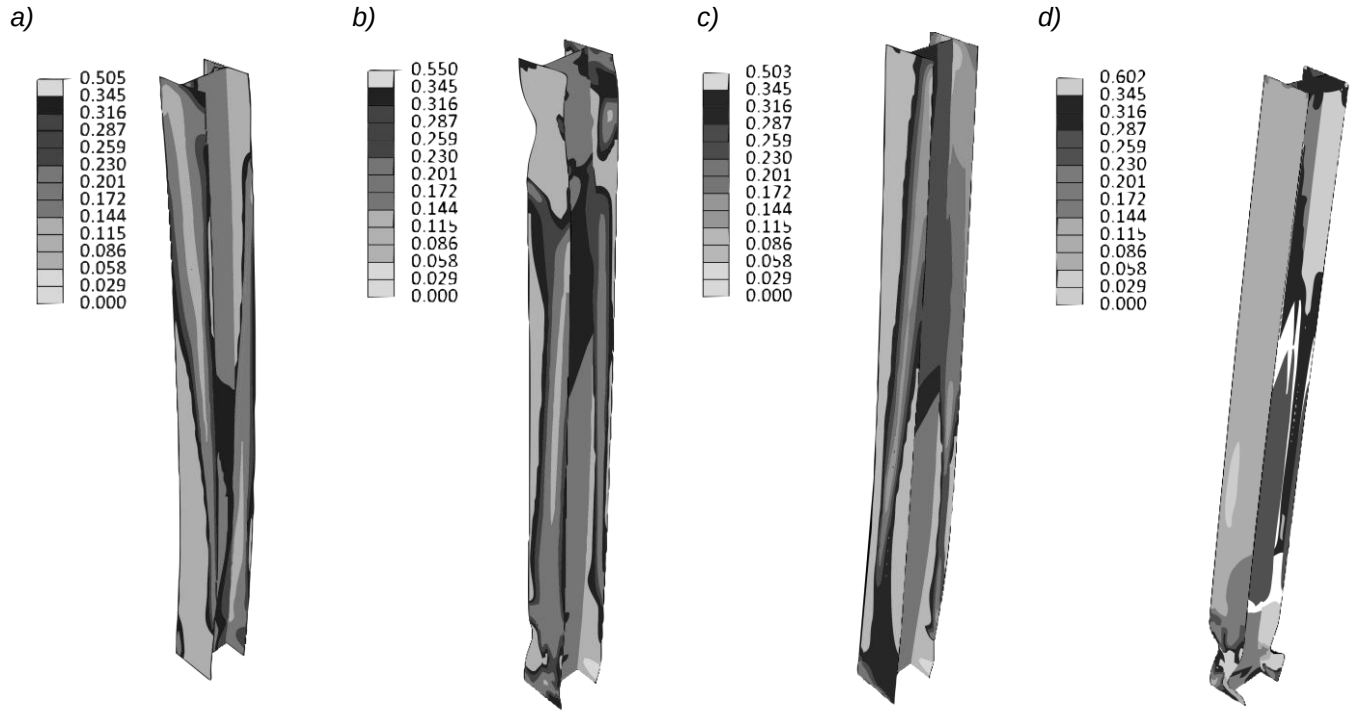

Figure 2. Von Mises stress distributions (in kN/mm^2) and failure modes of virtual specimens: a) W310×129-Cont (failed by member buckling at 1% drift ratio); b) W310×97-Cont (failed by local buckling near both ends at 1% drift ratio); c) W310×129-Var (failed by combined local buckling near the bottom end and member buckling at 6.7% drift ratio); d) W310×97-Var (failed by local buckling near the bottom end at 11% drift ratio).

Figure 4a and 4b show axial shortening – drift ratio responses of the virtual specimens. The sign is negative when the column is shortened. As shown the amplitudes of axial shortening at the end of the analysis vary between 0.75 and 2.25%, suggesting that axial shortening is a function of the failure mode under cyclic loading (e.g., local buckling near the ends or member buckling) and loading protocol as confirmed in the past studies (MacRae *et al.*, 2009). Another interesting observation is that axial shortening of stocky (Class 1) columns are almost identical to that of slender (Class 3) specimens. However, axial shortening of Class 1 specimens is dominated by out-of-plane deformation developed due to flexural buckling, while Class 3 columns shorten mainly because of the combined effects of flange and web local buckling at the column ends and lateral deformation along the column height.

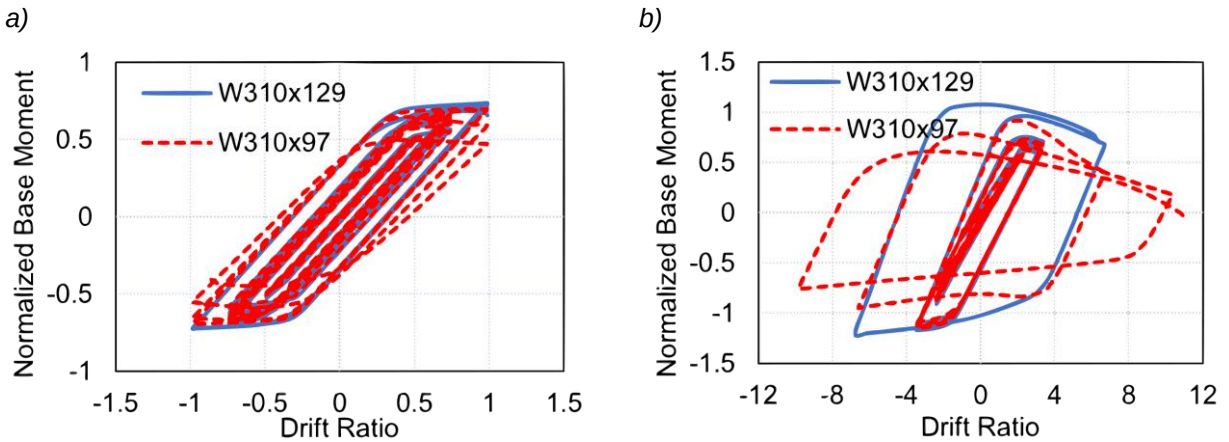

Figure 3. Moment vs. drift ratio response of the virtual specimens: a) Specimens under a constant axial load of P/P_n = 0.7 and AISC 341 strong axis displacement history (W310×129-Cont, W310×97-Cont); b) Specimens under varying axial load history with a maximum value of P/P_n = 0.7 and varying strong axis displacement and rotation history (W310×129-Var, W310×97-Var).

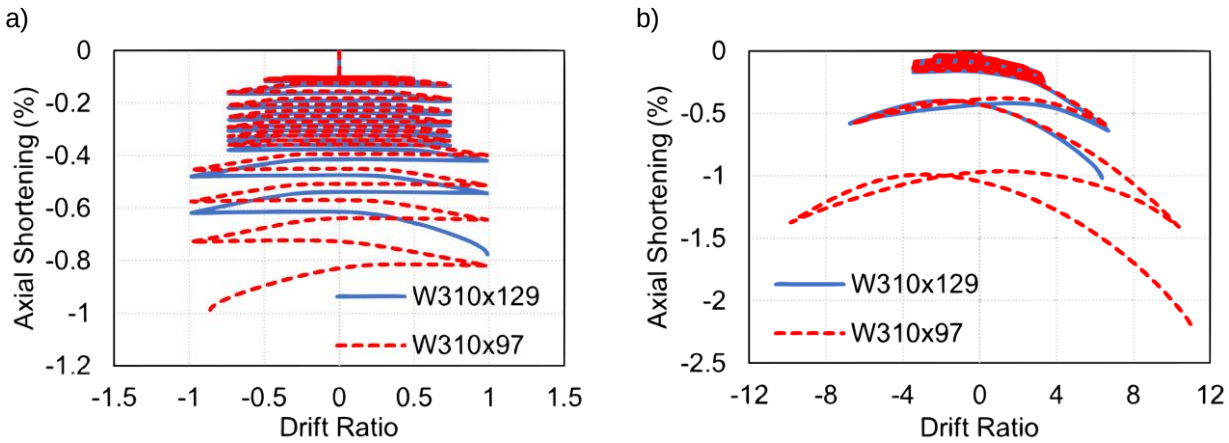

Figure 4. Axial shortening vs. drift ratio response of the virtual specimens: a) Specimens under a constant axial load of P/P_n = 0.7 and AISC 341 strong axis displacement history (W310×129-Cont, W310×97-Cont); b) Specimens under varying axial load history with a maximum value of P/P_n = 0.7 and varying strong axis displacement and rotation history (W310×129-Var, W310×97-Var).

4 Modelling challenges

Available nonlinear modelling approaches, including the concentrated plasticity approach and distributed plasticity technique, may not adequately capture the inherent cyclic inelastic response of steel CBF columns and their associated instability modes, particularly when columns do not meet member or section slenderness ratios implicit in contemporary building codes (ASCE, 2017; Balazadeh Minouei et al., 2017; Toutant et al., 2017). In the absence of numerical modelling techniques that systematically account for the nonlinear cyclic response of CBF columns, the available concentrated plasticity-based model adapted for wide-flange columns of steel MRFs can be used. This approach consists of two flexural plastic hinges located at two ends of the member connected using an elastic column (Lignos *et al.*, 2019). The properties of plastic hinges vary with respect to the constant axial force in the member. This approach however fails to explicitly account for three key response characteristics of CBF columns: 1) influence of varying axial load on the moment – rotation backbone curve, 2) interaction between axial shortening and moment – rotation response (MacRae, 1989; MacRae *et al.*, 2009); and 3) location of the flexural plastic hinges expected near the ends and along the length of the member where the moment, including second-order effects, is maximum. Despite these three limitations, the concentrated plasticity approach is adapted here for nonlinear analysis of steel CBF columns of Table 1 and later (in Section 5) recommendations are proposed to overcome these limitations in future.

The virtual specimens described in Section 2 are numerically modelled here using the available axial – moment concentrated plasticity model in SAP2000 version 21.2.0 (CSI, 2021), *Interacting P-M3*. This model accounts for 1) increased flexural moment capacity beyond yielding, 2) strength and stiffness degradation after moment

reaches its maximum value, 3) residual strength after a significant strength drop, 4) interaction between axial force and bending moment assuming that the axial force will remain constant during loading, and 5) axial force – axial displacement relationship proportional to moment – rotation response. It should be noted that the detailed description and respective formulations connecting axial shortening to moment – rotation response in the inelastic range is unavailable.

The concentrated plasticity-based model (CPM) developed in SAP2000 was used to perform three case studies: 1) W310×129-Cont failed by flexural (member) buckling, under monotonic loading, 2) W310×129-Cont failed by flexural buckling, under cyclic loading and 3) W310×129-Var failed by combined flexural buckling and local buckling near the ends under cyclic loading. The results from the detailed finite element model of the virtual specimens, as described in Section 2, were used to verify the response calibrated using the CPM in SAP2000.

The *interacting P-M3* hinges located at both ends of the CPM are first calibrated to reproduce the envelope of cyclic response of the specimen, as shown in Figure 5a for W310×129-Cont. As illustrated in Figure 5b, the calibrated CPM however fails to properly envelopes the axial shortening of the column under cyclic loading.

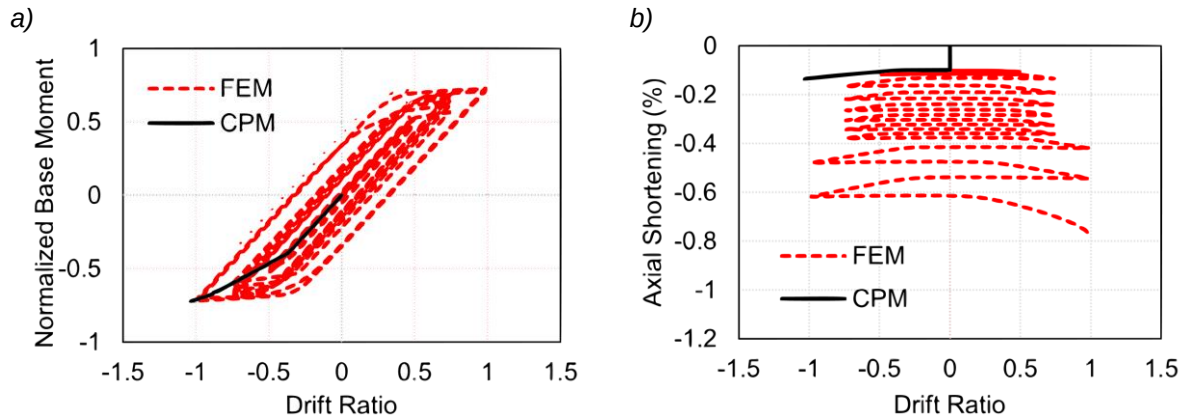

Figure 5. W310×129-Cont virtual specimen: a) Monotonic response calibration of CPM using moment – drift ratio response under cyclic loading; b) CPM prediction of axial shortening using the calibration in a).

The applicability of the CPM approach is then evaluated using a nonlinear time history analysis. Figure 6a and 6b compare the base moment and axial shortening of W310×129-Cont from the CPM against those predicted by the FEM, respectively. For this analysis, the *P-M3* hinges were calibrated to match the cyclic response of the column from the FEM and CPM. A very good correlation was achieved between two modelling techniques for the moment – drift ratio response, despite the complex stability response of the selected column. However, axial shortening is amplified by the CPM during cyclic loading. The peak axial shortening at the end of the analysis is almost 1.16 that anticipated using the FEM, suggesting that the adapted formulation that relates axial force – deformation response of the column to its moment – rotation response may not properly capture the complex nonlinear relationship between these response indicators.

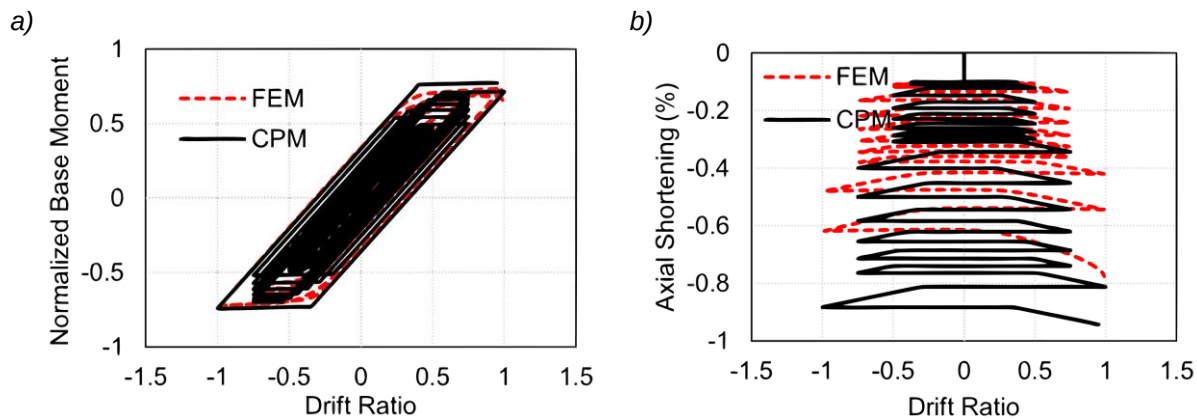

Figure 6. W310×129-Cont virtual specimen: a) Cyclic response calibration of CPM using moment – drift ratio response under cyclic loading; b) CPM prediction of axial shortening using the calibration in a).

The third case study involves the W310×129-Var column subjected to varying axial load plus strong axis lateral displacement at top and rotation at both ends as obtained from the cyclic pushover analysis of the CBF described earlier. Figure 7a and 7b show the moment – drift ratio and axial shortening – drift ratio responses of this specimen as obtained from the FEM and CPM developed here. Referring to Figure 7, the cyclic behaviour of W310×129-Var, including peak strength, strength and stiffness degradation, and axial shortening, was well calibrated by the numerically-efficient CPM. The negative post-yielding slope in the upper left corner of the plot stems from the detrimental effects of axial compression load acting on the deformed column on its moment capacity (P-Delta effects). Although a promising prediction was achieved by CPM for this loading scenario, these observations and findings must be interpreted with caution given that the relationship incorporated to translate moment – rotation response to axial force – axial deformation response has yet to be fully comprehended and thoroughly researched. For example, it is likely that the relationship between the axial force – deformation and moment – rotation response is linear, which is deemed to be unrealistic for CBF columns experiencing the sudden drop in axial deformation due to member buckling or combined flexural buckling and local buckling modes.

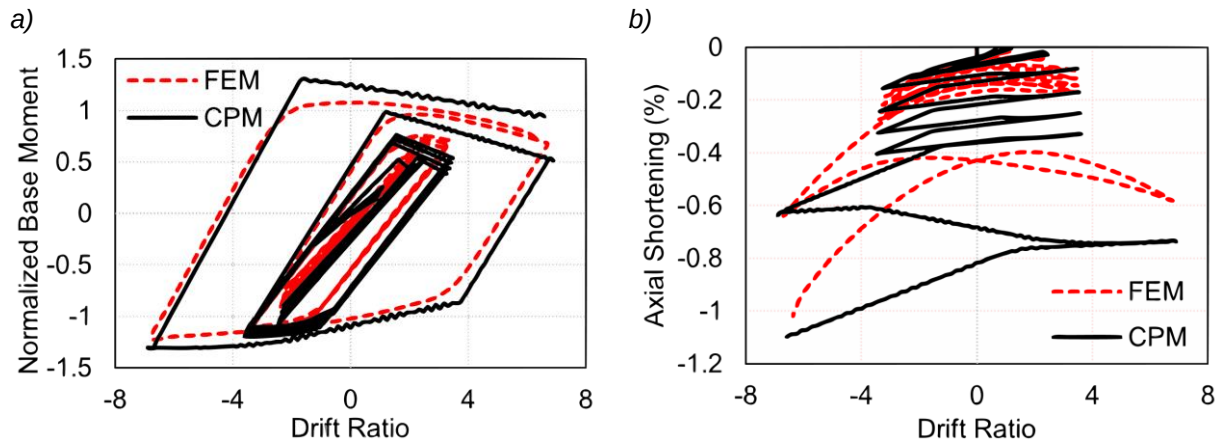

Figure 7. W310×129-Var virtual specimen: a) Cyclic response calibration of CPM using moment – drift ratio response under cyclic loading; b) CPM prediction of axial shortening using the calibration in a).

5 Future development

Several past studies attempted to develop empirical equations or numerical modelling techniques to predict axial shortening in wide-flange columns failing due to local buckling near the ends (MacRae *et al.*, 2009; Suzuki and Lignos, 2017; Elkady and Lignos, 2018). On the basis of observed cyclic response of steel wide-flange columns part of CBF structures, a first-cycle envelope curve relating axial shortening to drift ratio is proposed to be used in nonlinear static analysis of new and existing steel CBF columns (ASCE, 2017). This backbone curve is expected to inherently trace cyclic deterioration of steel wide-flange columns experiencing local buckling, global buckling, and combined local and global buckling. Figure 8 and Figure 9 show four examples of the proposed first-cycle envelope curves for the selected virtual specimens under constant and varying loading histories, respectively. Net axial shortening in plots refers to axial shortening minus the effects of the rigid body rotation of the column. In keeping with the simplicity of the CPM often used for nonlinear modelling of steel structures, the axial shortening first-cycle envelope curve should be used in conjunction with flexural first-cycle backbone curve to account explicitly for the interaction between the axial force, flexure – rotation and axial shortening – rotation.

A potential technique to implement this approach would be using a nonlinear translational spring located along the length of the member to simulate column axial shortening in conjunction with two rotational spring encompassing flexural first-cyclic envelope curve of the column. The proposed axial shortening first-cycle envelope curves should be adjusted for the applied axial compression load under a constant axial load case and the maximum applied axial load under varying axial compression load case, similar to moment – rotation backbone curves varying with the axial load level.

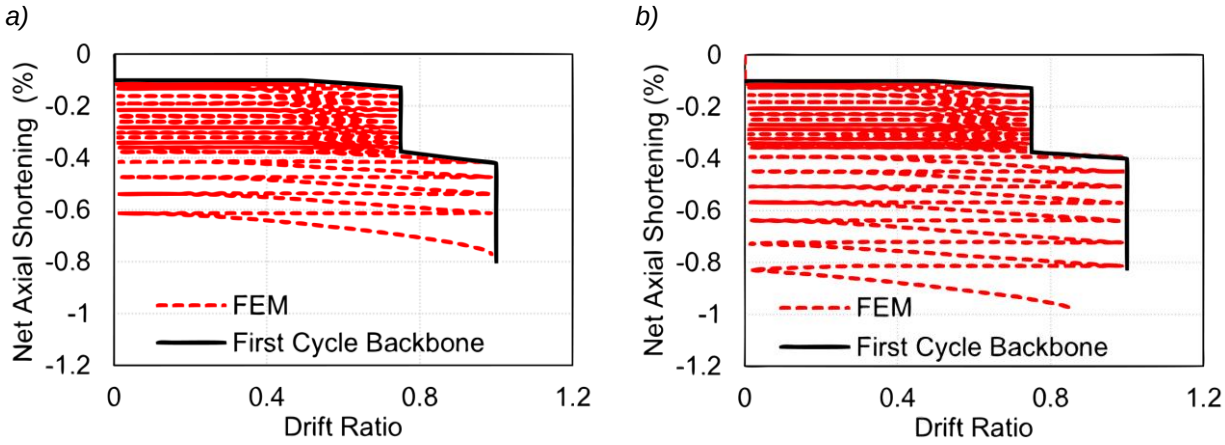

Figure 8. Axial shortening backbone curves of the virtual specimens: a) W310×129-Cont; b) W310×97-Cont.

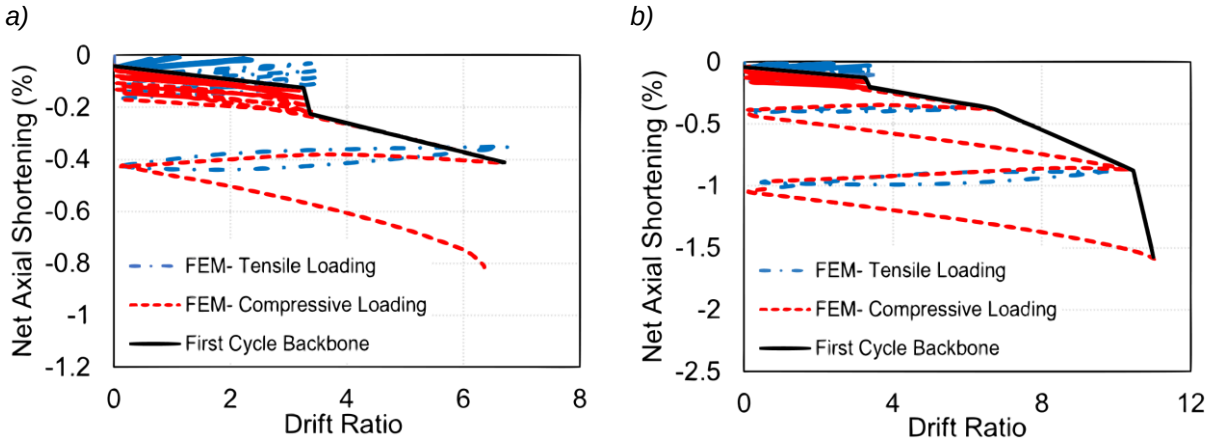

Figure 9. Axial shortening backbone curves of the virtual specimens: a) W310×129-Var; b) W310×97-Var.

An alternative approach to simulate inelastic cyclic response of steel wide flange columns in CBF structures would involve fibres with the material that accounts for flexural yielding and local buckling in the presence of axial force and incorporates axial shortening due to local and global buckling based on empirical equations developed using the past experimental data. Such fibre sections would only be located near the base, representing end flexural plastic hinges, and within the height of the column where the moment, including the second order effect, is expected to reach its maximum value, e.g., near the mid-height of the column (Balazadeh Minouei, 2017). The Fibres associated with the hinges are intended to simulate concomitantly moment – rotation and axial shortening – rotation responses in the presence of axial load.

6 Conclusion

This paper assessed the sufficiency of the concentrated plasticity-based nonlinear modelling approach for the simulation of the stability response of steel wide-flange columns in CBF structures, highlighted modelling challenges, and propose recommendations for future development of numerical modelling techniques to systematically simulate the local and global buckling modes of such columns plus their associated axial shortening. Two wide flange column specimens were selected, and their cyclic response was predicted using corroborated finite element model. Two loading protocols were considered: 1) constant axial force and AISC 341 symmetric cyclic displacement history in strong axis, and 2) varying axial load and varying lateral displacement and rotation in strong axis, which are obtained from cyclic pushover analysis of a 10-storey CBF structure. The selected column specimens were then analysed using a concentrated plasticity-based model developed in SAP2000 based on common modelling techniques often used in performance-based seismic engineering for nonlinear simulation of structures. The results of these simulations were used to make recommendations to enhance current state-of-practice in seismic assessment of steel structures in future. The key observations and findings of this study are as follows:

- The concentrated plasticity-based model incorporates several key features, including increased flexural moment capacity beyond the yielding point, strength and stiffness degradation beyond the capping strength, residual strength, consideration of interaction between axial force and bending moment while assuming constant axial force during loading, and a linear correlation between force – axial displacement response and moment – rotation response.
- The concentrated plasticity-based model can predict the moment – rotation response of wide flange column under a constant axial load and symmetric cyclic displacement, but axial shortening was over-predicted during cyclic loading. The cyclic behaviour of the selected wide flange column subjected to varying axial load and lateral displacement was well predicted using the numerically-efficient concentrated plasticity-based model.
- Despite the relatively accurate prediction of the column cyclic response by the concentrated plasticity-based model, the underlying formulation may not be fully applicable to the stability response of CBF columns under seismic loading. Therefore, the concentrated plasticity-based model used in this study should not be broadly applied for general engineering practice due to current challenges and associated concerns with such models.
- A potential method to complement the concentrated plasticity-based modelling approach and improve current state-of-the-art of nonlinear simulation for performance-based seismic engineering is to implement a first-cycle envelope curve relating net axial shortening to the drift ratio for steel wide flange columns of CBF structures. Both axial shortening and flexural backbone curves vary with respect to the axial load level in the member. The proposed technique once implemented can facilitate nonlinear static analysis of new and existing steel CBF columns.

7 Acknowledgements

Acknowledgment is extended for the financial support received from the Natural Sciences and Engineering Research Council (NSERC) of Canada through the Discovery Grant Programs. The authors wish to express their gratitude to the University of Alberta Centre for Steel Education and Research (The Steel Centre) for their support.

8 References

Simulia, D.S. (2020). “Abaqus/ CAE”, *Dassault Systemes Simulia Corporation*, Johsnton, RI, USA.

Altair Engineering INC (2023). “Altair S-FRAME”, *Altair Engineering INC*, Troy, MI, USA.

ANSI/AISCa (2022). *“Seismic Provisions for Evaluation and Retrofit of Existing Structural Steel Buildings (ANSI/AISC 342-22)”*, *AISC*, Chicago, IL, USA.

ANSI/AISCb (2022). “*Code of standard practice for steel buildings and bridges (ANSI/AISC 303-22)*”, AISC, Chicago, IL, USA.

ANSI/AISCc (2022). “*Specification for structural steel buildings (ANSI/AISC 360-22)”*, *AISC,* Chicago, IL, USA.

ANSI/AISCd (2022). “Seismic Provision for Structural Steel Buildings (ANSI/AISC 341-22)”, *AISC*, Chicago, IL, USA.

ASCE (2017). “Seismic Evaluation and Retrofit of Existing Buildings (ASCE 41-17)”, *ASCE*, Reston, VA, USA.

ASTM (2021). “*Standard specification for general requirements for rolled structural steel bars, plates, shapes, and sheet piling (ASTM A6/A6M)”*, *ASTM*, West Conshohocken, PA, USA.

Auger, K. (2017). “Conception parasismique des contreventements concentriques en treillis à segments multiples combinés aux poteaux gravitaires”, *Ecole Polytechnique,* Montreal, QC, CA.

Balazadeh Minouei, Y. (2017). “*Seismic Evaluation and Retrofit of Existing Concentrically Braced Steel Frames in Canada”*, *Ecole Polytechnique*, Montreal, QC, CA.

Balazadeh Minouei, Y., Koboevic, S. and Tremblay, R. (2017). “Seismic evaluation of a steel braced frame using NBCC and ASCE 41”, *Journal of Constructional Steel Research*, 135, pp. 110–124.

Cravero, J., Elkady, A. and Lignos, D.G. (2020). “Experimental evaluation and numerical modeling of wide-flange steel columns subjected to constant and variable axial load coupled with lateral drift demands”, *Journal of Structural Engineering*, 146(3), p. 04019222.

CSA (2019), "Design of Steel Structures (CSA S16: 19)", Canada Standards Association, *National Standard of Canada*, Toronto, ON, CA.

CSI Analysis (2021). "SAP2000- 21.2.0", *Computers & Structures, INC*, Walnut Creek, CA, USA:.

CSI Analysis (2023). "ETABS", *Computers & Structures INC*, Walnut Creek, CA, USA.

Dlubal Software, Inc. (2023). "RFEM 6 | FEM Structural Analysis Software", *Dlubal Software, Inc*, Philadelphia, PA, USA.

Elkady, A. (2016). "Collapse risk assessment of steel moment resisting frames designed with deep wide-flange columns in seismic regions", *McGill University*, Montreal, QC, CA.

Elkady, A. and Lignos, D.G. (2018). "Full-scale testing of deep wide-flange steel columns under multiaxis cyclic loading: Loading sequence, boundary effects, and lateral stability bracing force demands", *Journal of Structural Engineering*, 144(2), p. 04017189.

Fogarty, J. and El-Tawil, S. (2016). "Collapse resistance of steel columns under combined axial and lateral loading", *Journal of Structural Engineering*, 142(1), p. 04015091.

Hartloper, A.R., de Castro e Sousa, A. and Lignos, D.G. (2021). "Constitutive modeling of structural steels: nonlinear isotropic/kinematic hardening material model and its calibration", *Journal of Structural Engineering*, 147(4), p. 04021031.

Lamarche, C.-P. and Tremblay, R. (2011). "Seismically induced cyclic buckling of steel columns including residual-stress and strain-rate effects", *Journal of Constructional Steel Research*, 67(9), pp. 1401–1410.

Lemaitre, J. and Chaboche, J.L. (1990). "Mechanics of Solid Materials", *Cambridge University Press,* Cambridge, United Kingdom.

Lignos, D.G. *et al.* (2019). "Proposed updates to the ASCE 41 nonlinear modeling parameters for wide-flange steel columns in support of performance-based seismic engineering", *Journal of Structural Engineering*, 145(9), p. 04019083.

MacRae, G.A. (1989). "The seismic response of steel frames", *University of Canterbury, Christchurch, New Zealand.*

MacRae, G.A. *et al.* (2009). "Axial shortening of steel columns in buildings subjected to earthquakes", *Bulletin of the New Zealand Society for Earthquake Engineering*, 42(4), pp. 275–287.

Newell, J.D. and Uang, C.-M. (2008). "Cyclic behavior of steel wide-flange columns subjected to large drift", *Journal of structural engineering*, 134(8), pp. 1334–1342.

Seki, A. *et al.* (2022). "Seismic performance of steel chevron braced frames designed according to Japanese practice", *Journal of Constructional Steel Research*, 189, p. 107066.

Suzuki, Y. and Lignos, D. (2017). "Collapse behavior of steel columns as part of steel frame buildings: Experiments and numerical models", in *Proceedings of the 16th World Conference on Earthquake Engineering (16WCEE)*, International Association of Earthquake Engineering.

Toutant, G. *et al.* (2017). "Stability of steel columns in steel concentrically braced frames subjected to seismic loading", in *Structures Congress 2017*, pp. 143–154.